MDPI

Article

Pyrometallurgical Lithium-Ion-Battery Recycling: Approach to Limiting Lithium Slagging with the InduRed Reactor Concept

Stefan Windisch-Kern * [iD], **Alexandra Holzer, Christoph Ponak** [iD] **and Harald Raupenstrauch**

Chair of Thermal Processing Technology, Montanuniversität Leoben, Franz-Josef-Strasse 18, 8700 Leoben, Austria; alexandra.holzer@unileoben.ac.at (A.H.); christoph.ponak@unileoben.ac.at (C.P.); harald.raupenstrauch@unileoben.ac.at (H.R.)
* Correspondence: stefan.windisch-kern@unileoben.ac.at

Abstract: The complexity of the waste stream of spent lithium-ion batteries poses numerous challenges on the recycling industry. Pyrometallurgical recycling processes have a lot of benefits but are not able to recover lithium from the black matter since lithium is slagged due to its high oxygen affinity. The presented InduRed reactor concept might be a promising novel approach, since it does not have this disadvantage and is very flexible concerning the chemical composition of the input material. To prove its basic suitability for black matter processing, heating microscope experiments, thermogravimetric analysis and differential scanning calorimetry have been conducted to characterize the behavior of nickel rich cathode materials ($LiNi_{0.8}Co_{0.15}Al_{0.05}O_2$ and $LiNi_{0.33}Mn_{0.33}Co_{0.33}O_2$) as well as black matter from a pretreatment process under reducing conditions. Another experimental series in a lab scale InduRed reactor was further used to investigate achievable transfer coefficients for the metals of interest. The promising results show technically feasible reaction temperatures of 800 °C to 1000 °C and high recovery potentials for nickel, cobalt and manganese. Furthermore, the slagging of lithium was largely prevented and a lithium removal rate of up to 90% of its initial mass was achieved.

Keywords: lithium-ion-batteries; pyrometallurgical recycling; carbothermal reduction

1. Introduction

Since 1979, when Goodenough et al. finally tested $LiCoO_2$ (short: LCO) as a cathode material, the development and commercialization of electrochemical energy storage based on the lithium-ion technology has been steadily pushed forward [1,2]. Lithium-ion-batteries (LIBs) basically consist of the same components such as anode, cathode, separator or electrolyte as can be found in other battery technologies. This basic principle has not changed since 1979 and therefore also applies to modern LIBs. However, the initially used LCO cathode material is now just one option on a long list of alternatives like NCA ($LiNi_xCo_yAl_zO_2$), NMC ($LiNi_xMn_yCo_zO_2$) or LFP ($LiFePO_4$) materials [3]. The variety of cathode materials is not only based on the fields of possible applications that reach from mobile electronics to e-mobility or stationary storages and their respective demand for performance (energy and power density) or safety aspects, but also on factors like raw material prices, supply risks or social and ecological sustainability. Concerning the development of the LIB market numerous publications can be found. Especially the electric automotive sector will benefit from decreasing costs made possible by mass production and optimized cell chemistry. Berckmans et al. [4] states that by 2030, the cut of fully electric or hybrid vehicles will rise to 25% of the total vehicles sold. In view of the high amount of valuable metals that are contained in LIBs, especially in their cathode materials, and the predicted market demand [5], an efficient recycling process in order to recover the mentioned valuable metals is absolutely necessary.

In general, the recycling of LIBs can be divided into three processing steps, namely pretreatment, metal extraction and metal refining. The recycling chain of LIBs usually starts

with pre-treatment processing which aims to separate battery components like the battery management system or the housing and the corresponding materials such as plastics or iron from the active materials of the battery electrodes. For pre-treatment, various processes can be found which differ more or less from each other. Basically, steps during pre-treatment are sorting, dismantling deactivation and mechanical processing and separating. Said active materials–after pre-treatment they are also known as black matter–mainly consist of lithium metal oxides or lithium iron phosphate, carbon and residues from the electrode conductor foils. Umicore's Valéas process, for example, is an exception since it does not need a usual pre-treatment but uses the batteries directly in their pyrometallurgical process. [2,6–12].

While the obtained metal and plastic scrap can be recycled directly, the produced black matter that contains the valuable metals needs to be further treated in a metal extraction step to recover Li, Ni, Co and Mn, at best in a quality that is suitable for closed loop recycling. Therefore, pyro-, bio- and hydrometallurgical methods can be used. Biometallurgical processes like bioleaching are considered as environmentally friendly and low cost alternatives to conventional hydrometallurgy, capable of reaching recovery rates of more than 98% for Ni and Co and more than 80% for Li but suffering from low kinetics and resulting poor throughput rates [13–19].

Typical hydrometallurgical procedures, used to recover metals from black matter, are leaching, solvent extraction, chemical precipitation or electrochemical deposition, with which a high selectivity and therefore product purity can be achieved [20]. The possible recovery rates for Ni, Mn, Co and Li, as for example reported by He et al. [21], can be close to or even higher than 99%. The obtained salts or concentrates can usually be directly used for the production of new cathode materials as it is the case for the Duesenfeld process described by Elwert and Frank [22]. An indication of the importance of hydrometallurgical recycling of spent LIBs is, among other things, the high intensity of research activities in this field. According to Huang et al. [23], more than half of the recycling processes that are currently under investigation are related to hydrometallurgical processing.

Pyrometallurgical approaches use high temperatures, usually above 1400 °C, and reducing conditions to recover valuable metals as a metal alloy. The advantages lie in the experience with and the properties of conventional pyrometallurgical units which are less complex and less vulnerable, e.g., to organic impurities in the black matter, than their hydrometallurgical counterparts. The decisive factor in this regard is the oxygen potential of the contained metals, which is for example low for Ni and Co, leading to a relatively low-effort recovery. On the other hand, the similarity of the oxygen potential between Ni and Co reduce the selectivity of pyrometallurgical processes since they cannot be recovered separately but only as an alloy. The oxygen potential is also responsible for one of the biggest disadvantages of pyrometallurgy. Lithium, which has a much higher oxygen affinity, cannot be recovered as part of the metal alloy but is bound as an oxide in the slag instead [2,20,24–26].

The refining step is usually based on hydrometallurgical methods and aims for a closed loop recycling. Hence, it mainly applies on the metal alloy and slag from pyrometallurgical processing, which without further treatment, cannot be used for the production of new LIBs. The treatment of the metal alloy aims for a separation of the contained metals, while the slag treatment's goal is to recover Li, which is often technically but not economically feasible due to the low Li content in the slag. [2,20,22,27]

However, it can be summarized that there are still a lot of uncertainties in the LIB recycling chain. Not only the development of the waste stream itself, also the number and diversity of pre-treatment processes lead to varying black matter compositions and qualities. For pyrometallurgy, the lack of Li recovery options is a major problem that is not yet solved, but however, gives the desired novel approach with the InduRed reactor a good opportunity to establish itself as an alternative to conventional processes.

The mentioned InduRed reactor might be a possibility to achieve a simultaneous recovery of Ni, Co, Mn as well as Li with a pyrometallurgical process. The existing pilot-scale reactor concept, shown in Figure 1a,b, consists of a packed bed of graphite pieces that

is inductively heated by surrounding copper coils. The input material is fed continuously with up to 10 kg/h from the top onto the hot graphite bed. The uppermost induction coil powers the upper third of the reactor where the input material melts and forms a thin molten layer that moves downwards. A second induction coil, placed half way down the reactor, induces enough power so that reduction reactions can take place. Gaseous reaction products are then removed from the reactor via a flue gas pipe whereas the liquid products move further down. The third induction coil makes sure that the temperature within the reactor can be maintained well above the melting temperature of the mixture and enables a continuous flow out of the bottom of the reactor. The advantages of the reactor are the low oxygen partial pressure, the possibility to control different temperature zones, and the big reaction surface due to the graphite bed. Furthermore, the contact time and intensity between gaseous reaction products and the molten phase can be limited because they only need to pass a thin layer or droplets instead of a molten bath like in conventional pyrometallurgical furnaces. Originally, the reactor concept was developed for the recovery of phosphorus from sewage sludge ashes, which is described by Schönberg [28]. The concept was later also adapted by Ponak et al. [29,30] to treat basic oxygen furnace slag with limited iron phosphide formation.
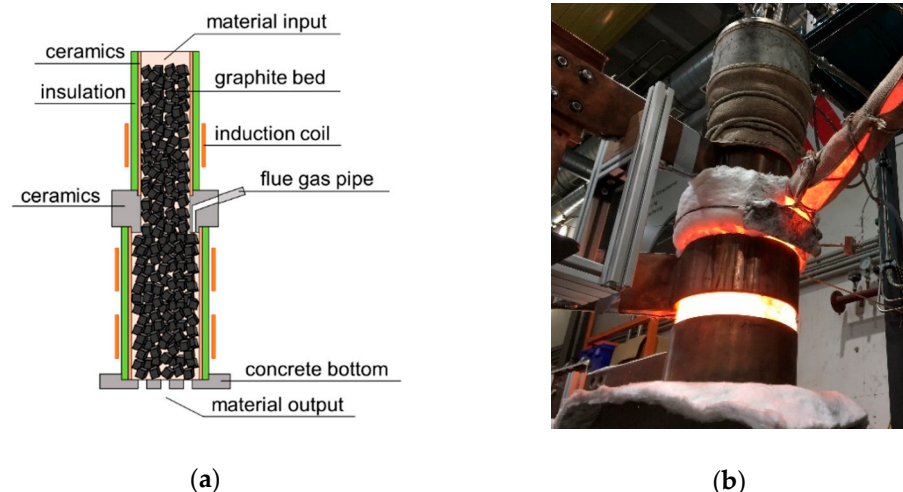

(**a**)　　　　　　　　　　　　　　　　　　(**b**)

Figure 1. (**a**) Schematic illustration of the so called InduRed reactor and (**b**) said reactor operating at a test series for metal recovery from basic oxygen furnace slag. [29,30].

The aim of this work is to investigate if said reactor concept can potentially also provide a solution for LIB black matter recycling.

For the determination of the basic suitability of black matter as an input material for the InduRed reactor, thus its melting and reaction behaviour, heating microscope experiments, thermogravimetric analysis (TGA) and differential scanning calorimetry (DSC) were carried out. Since black matter can have different properties and contents of impurities depending on the pre-treatment procedure, the influence of which on the properties being investigated is difficult to assess, the investigations are also carried out with pure cathode materials. The ability of the InduRed reactor concept to eliminate one of the biggest disadvantages of pyrometallurgical LIB recycling, namely lithium slagging, is finally evaluated by experiments in a lab-scaled batch reactor, which is based on the InduRed concept. The results, in particular the required reaction temperatures and the Li removal rate via the gas phase from the reactor, form the basis on which a decision is made about the fundamental suitability of the reactor to be part of the LIB recycling chain.

2. Materials and Methods

The cathode materials ($LiNi_{0.8}Co_{0.15}Al_{0.05}O_2$, sample abbreviation: NCA and $LiNi_{0.33}Mn_{0.33}Co_{0.33}O_2$, sample abbreviation: NMC) which were used for the experiments have

been produced by Gelon Energy Corporation in Linyi, China, while the black matter (sample abbreviation: AM) was provided by a LIB recycling facility operated by Redux GmbH in Bremerhaven, Germany. The chemical composition of said materials is summarized in Table 1 below.

Table 1. Chemical composition of used materials. (mass fraction, w/%).

Species	C	Li	Ni	Co	Mn	Al	P	Fe	Cu	Zn	Pb
AM [1]	29.5	2.4	20.9	4.2	1.1	5.8	0.4	0.6	5.7	0.8	0.1
NCA [2]	-	7.2	48.9	9.2		1.4					
NMC [2]	-	7.2	20.3	20.4	19.0	-					

[1] Data from ICP-MS analysis. [2] Calculated from the molar composition of the cathode materials.

In experiments with NCA and NMC, where reducing conditions were desired (sample abbreviation: NCA_C, NMC_C), fine powdered coke was used as a reducing agent. Since AM already contains 29.5 w/% carbon there was no need to further add a reducing agent.

In order to investigate the general behavior of the cathode materials at high temperatures and under reducing conditions, the work started with two preliminary experimental series. First, heating microscope experiments were conducted in a Hesse Instruments EM 201 with an HR18-1750/30 furnace (Hesse Instruments, Osterode am Harz, Germany) to investigate at which temperatures reactions or transformations in the sample occur. In the heating microscope experiments, black matter and the cathode materials with and without carbon addition were tested at least twice to check the reproducibility of the results. In the reduction experiments, carbon was added in extents of 10 w/% to the NCA and NMC materials. An argon purge with a flow rate of approximately 2.5 l/min was used to inhibit oxidization reactions of the materials. The settings for the heating rate (80 °C/min until 1350 °C, 50 °C/min until 1550 °C and 10 °C/min until 1650 °C with a holding time of 5 min at 1650 °C), the used Al_2O_3 sample plates and the sample size of approximately 0.1 g of powder, pressed in a cylindrical shape, were the same for all experiments.

The second series were simultaneous thermal analyses (STA), more precisely thermogravimetric analysis (TG) and differential scanning calorimetry (DSC), which have been conducted in a Setaram Setsys Evo 2400 at the Chair of Physical Metallurgy and Metallic Materials at the Montanuniversitaet Leoben. The aim of the STA was to confirm the temperature zones in which changes of the materials could be observed in the heating microscope and to further characterize the underlying reaction mechanisms. An argon purge was used to inhibit oxidization reactions of the materials. For carrying out the analyses, graphite crucibles and a carbon addition of 25 w/% were used in order to prevent damages to the analysis hardware. The need for this is due to reactions between standard Al_2O_3 crucibles and the produced metal alloy when carbon is added to the mixture. The reactions lead to a destruction of the Al_2O_3 crucible and the thermocouple underneath gets destroyed. The higher amount of carbon in the STA experiments is needed to prevent reactions between the cathode material and the graphite crucible, which would take part as a reductant.

To simulate the conditions of the InduRed reactor and check its suitability, a third set of experiments has been performed in the so-called InduMelt plant (sample abbreviation starts with: IM_). The InduMelt plant is a single coil induction furnace that is modeled on the InduRed reactor concept and used to perform preliminary experiments. This is due to the fact that the InduMelt plant is easier to use and requires less effort compared to the continuous InduRed reactor but still provides the same reaction conditions. The crucible concept used for these experiments is therefore based on the InduRed reactor and consists of a bed of packed graphite cubes (25 mm edge length) within an Al_2O_3 ceramics ring (70 mm radius, 100 mm height) and is shown in Figure 2a. In Figure 2b, the setup of the InduMelt plant is presented.
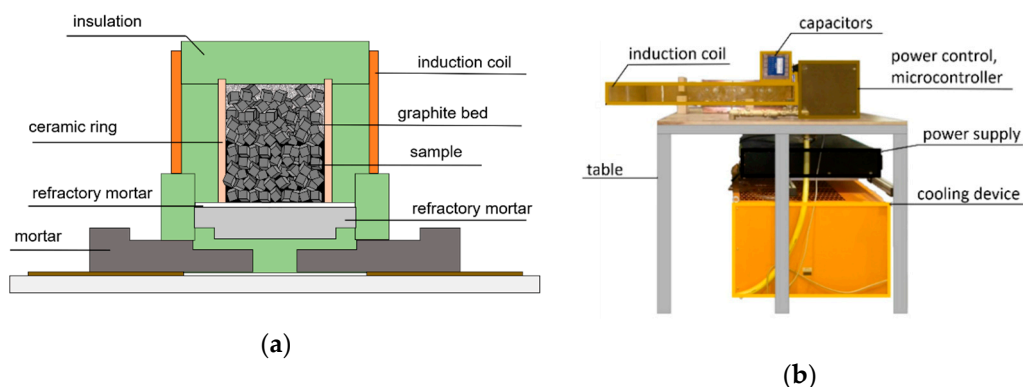
(**a**)

(**b**)

Figure 2. (**a**) Schematic illustration of the crucible concept used in the InduMelt experiments [29] and (**b**) setup of the experimental InduMelt plant.

During the preparation of the experiments, the ceramic ring is fixed on a mortar plate with refractory mortar and alternatingly filled with graphite cubes and input material. In the conducted experiments, the initial sample mass was 552.3 g for IM_NMC_C, 520.0 g for IM_NCA_C and 561.9 g for IM_AM. The filled crucible is then insulated, using 20 mm thick Cerachrome fiber wool with a classification temperature of 1500 °C and placed within the induction coil. The inductive energy input is controlled in such a way that the temperature increases at a maximum rate of 200 °C/h. For the measurement of temperatures of the reactor, two k-type thermocouples are used inside of the reactor to control temperatures up to 1200 °C. To keep track of the temperature after the k-type couples fail due to the high temperatures, two separate s-type couples are mounted on the outer wall of the Al_2O_3 ceramics ring. The temperature distribution in the reactor is known from previous experiments with other waste streams and can show a gradient of several 100 °C towards the end of the experiment, with the highest temperatures occurring at the top of the reactor. The s-type thermocouples are therefore placed at the lower third of the reactor in order to reach the necessary temperatures in the area in which the material is supposed to accumulate.

After the experiments, the reactor needs to cool down for at least 24 h before the sampling can start. Hereby, every graphite cube was picked from the reactor one after another and checked for any metal or slag depositions, which, if present, were removed from the cube's surface and collected. The difficulty to collect every little metal deposition and its influence on the overall mass balance of each experiment is discussed in the results section of this work.

However, representative samples were taken from the collected products and the content of species of interest was examined using inductively coupled plasma mass spectrometry (ICP-MS). For all ICP-MS measurements, which were conducted at the Chair of Waste Processing Technology and Waste Management at the Montanuniversitaet Leoben, the sample preparation was done by aqua regia digestion according to the ÖNORM EN 13657 standard. The measurement of the respective species was carried out according to the ÖNORM EN ISO 17294-2 standard.

3. Results

3.1. Heating Microscope

In the heating microscope experiments, the relative cross-sectional area (CSA) of the sample, thus the trend of cross sectional area of the sample cylinder during heating in relation to its initial value, was observed to investigate at which temperatures changes in the material occur. In Figure 3a, where the results of the test series with NMC are shown, one can see a significant difference between the graphs of NMC_1 and NMC_2 without carbon addition and, respectively, NMC_C_1 and NMC_C_2 in which carbon was added. In this case, the first change of the CSA for NMC_C_1 and NMC_C_2 can be observed at approx. 800 °C, which is almost 200 °C lower than in the tests without carbon addition.

Moreover, the extent to which the change occurs is significantly higher in experiments with carbon addition. The steep decline of NMC_C_1 and NMC_C_2 at approx. 1500 °C was also observed with other cathode materials and can be explained by the melting point of the contained metals. The difference in the trends of the CSA with and without carbon addition can be explained by the origin of the changes. Mao et al. [31] and Kwon and Sohn [32] investigated and described the reaction behaviour of LCO ($LiCoO_2$) with and without carbon addition. According to their findings and due to the fact, that NCA and NMC are structurally identical to LCO, we assume that the changes in experiments without carbon addition are caused by thermal decomposition of the lithium metal oxides, while in experiments with carbon addition, reduction reactions with Li_2O formation led to the observed changes. About the reproducibility it can be said that in the repeated attempts the characteristic changes of the CSA appear at the same temperatures to about the same extent.
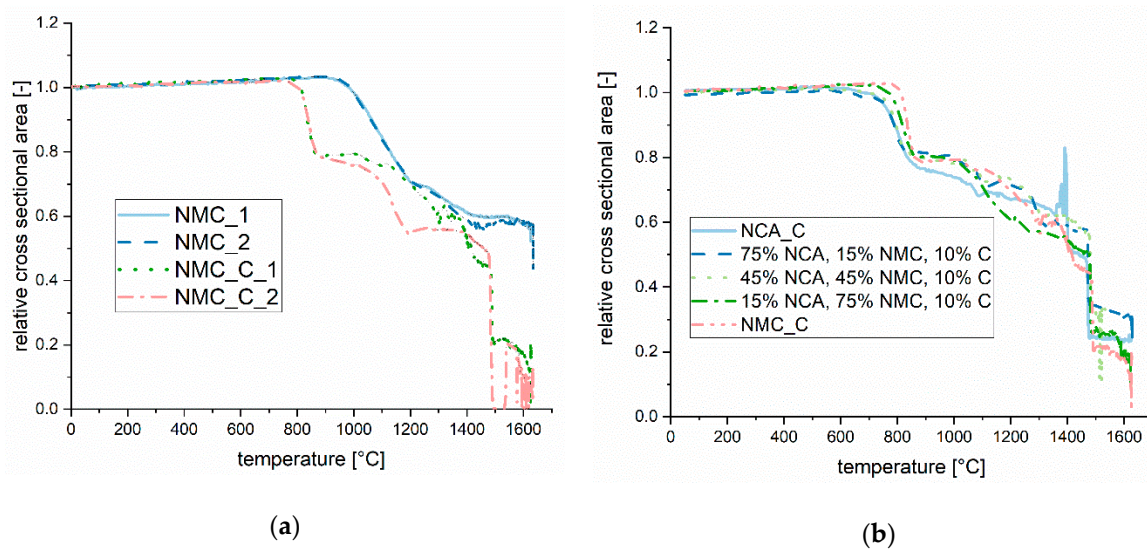

(**a**)

(**b**)

Figure 3. (**a**) Comparison of the cross sectional area of NMC with and without carbon addition in the heating microscope; (**b**) Comparison of the cross sectional area of different mixtures of NMC and NCA, each with carbon addition.

The results, mainly temperature zones and the extent of the correspondence of changes of the CSA, for NCA and NCA_C are very similar to those for NMC and NMC_C. However, since future waste streams are likely to consist of mixtures of different cathode materials, another set of experiments was performed in which NCA and NMC in different compositions and carbon were mixed to investigate if the materials influence each other. In Figure 3b, where the changes of the CSA of NCA_C, NMC_C and mixtures with varying composition are shown, no direct influence can be seen. The following Figure 4a,b show the NMC_C sample before and after the heating microscope experiment. In Figure 4b a perfectly molten metal sphere, indicated by the change of the CSA at approx. 1500 °C, and a fine white crystalline structure can be seen. The blue colour of the Al_2O_3 ceramic is most likely caused by reactions with cobalt and was also observed in all other experiments, especially in those with carbon addition.

(**a**) (**b**)

Figure 4. (**a**) NMC_C sample before and (**b**) after heating to 1600 °C in the heating microscope.

In contrast, the black matter material (AM) showed a completely different behavior, as can be seen in Figure 5a,b in which its CSA does not decrease during heating but increase to almost 120% of its initial value. The lack of the first change of the AMs CSA as well as the absence of any sign of melting at temperatures around 1500 °C indicates that pre-treatment might have a big influence on basic thermophysical properties of the produced black matter.
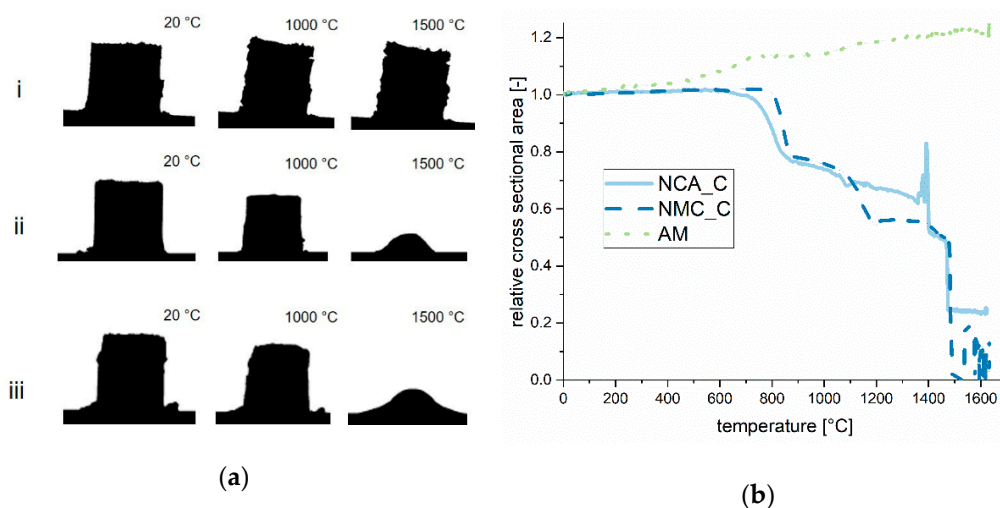

(**a**) (**b**)

Figure 5. (**a**) Images of the samples AM (i), NMC_C (ii) and NCA_C (iii) at temperatures of 20 °C, 1000 °C and 1500 °C taken during the heating microscope experiments; (**b**) Trend of the cross sectional area of the samples AM, NMC_C and NCA_C during heating in the heating microscope.

Reasons for the deviating behavior of AM compared to NMC_C and NCA_C could lie in impurities, thus residues from the mechanical processing and separation step during pre-treatment, like Cu and Al from conductor foils. A closer look at the chemical composition of AM in Table 1 reveals that the mass content of Cu and Al with almost 6% each is much higher than anticipated. Moreover, the carbon content is much higher than would be stoichiometrically necessary for the reduction reactions. An example of a disruptive reaction could be the formation of aluminum oxide which, in the appropriate amount, could form a supporting structure and thereby reduce the informative value of the CSA. On the other hand, it is also possible that the anode graphite has a lower reactivity than the fine powdered coke which is used in NMC_C and NCA_C.

The origin of AM, a pre-treatment process that uses thermal deactivation before mechanical shredding, could also cause the observed differences, since some of the reactions might already have taken place if certain temperatures are overcome during this step. By this, the layered structure of the lithium metal oxides could probably have been changed, e.g., due to thermal decomposition which, as can be seen in Figure 3, occurs at

approx. 1000 °C and could change the materials properties permanently. However, reliable information about these thermal processes is difficult to access. In our opinion, however, it is quite possible that at certain points in such a process, temperatures above 1000 °C can occur and that therefore the possibility of influencing the material must not be excluded.

3.2. Simultaneous Thermal Analysis

The experiments in the heating microscope gave some first impressions on how NMC, NCA and AM behave at high temperatures and under reducing conditions. For further characterization of the underlaying reactions that cause respective changes in the materials and to create a basis for a kinetics model in the long term, thermogravimetric analysis and differential scanning calorimetry was conducted. The results of the STA are summarized in Figure 6a, showing the trends of the relative mass of the samples, and Figure 6b, which shows the corresponding trends of the heat flow. The evaluation of the measurements, which also includes a correction of the data by reference measurements, was carried out in MATLAB.
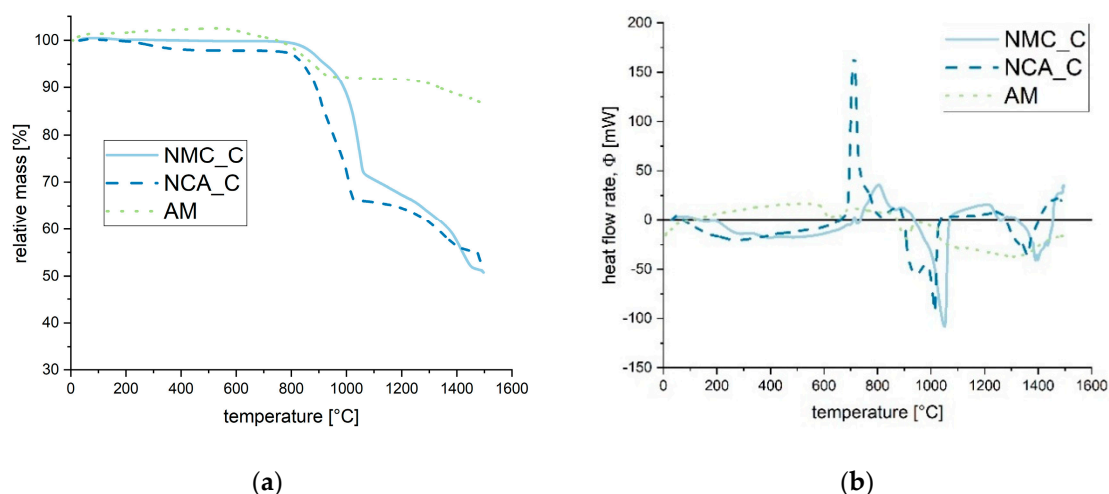

(**a**)   (**b**)

Figure 6. Results of the simultaneous thermal analyses of NMC_C and NCA_C with a heating rate of 40 K/min. (**a**) Trend of the relative mass of NMC_C and NCA_C during heating. (**b**) Trend of the heat flow of NMC_C and NCA_C during heating.

In Figure 6a the beginning of the mass loss at approximately 800 °C matches the observations from the heating microscope experiments. The first mass loss first declines slowly before it becomes steeper around 1000 °C and stops at approximately 70 % of the initial mass which was 40.1 mg for NCA_C and 39.8 mg for NMC_C. At the end of the thermogravimetric curve, the relative mass is about 55% of the initial mass. This means, that additionally to carbon, which had an initial mass content of 25 w/%, also components of the lithium metal oxide, most likely O_2 and Li, had been removed from the sample. Another indication for the presence of reduction reactions between 800 °C and 1000 °C is the trend of the heat flow, shown in Figure 6b. In both samples, the heat flow between 800 °C and approximately 1050 °C is endothermic with a negative peak around 1000 °C where also the biggest slope of the sample mass occurs. The outstanding exothermic peak in the NCA_C at 700 °C heat flow trend could be the result from Al_2O_3 formation whereby a significant amount of heat could be released. In order to confirm this, the samples must be heated in a controlled manner to or just above this temperature and analysed using XRD analysis, which is planned within the further scope of the research project.

As in the heating microscope experiments, the behaviour of the sample AM differs greatly from that of NCA_C and NMC_C. The overall mass loss only accumulates to around 10% and there are no sharp peaks in the heat flow trend. The lower mass loss is on the one hand due to the comparatively lower lithium metal oxide content (<60 w/%) compared to NCA_C and NMC_C (75 w/%) and the resulting decreased ability for CO or CO_2 generation. Since the heating rate was the same in all experiments, the less steep mass

loss between 800 °C and 1000 °C and the absence of significant peaks in the heat flow trend indicate a lower reactivity of AM in general. The suspicion from the heating microscope experiments that certain reactions already took place during the thermal deactivation step has gotten stronger.

Finally, the results from the heating microscope experiments and the STA are summarized in Figure 7.
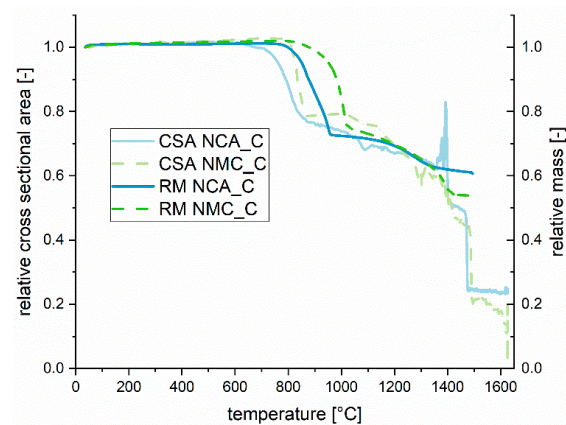

Figure 7. Trends of the cross-sectional area and the relative mass of NMC_C and NCA_C during heating in the heating microscope experiments and the simultaneous thermal analysis.

3.3. InduMelt Experimients

The last experimental series was conducted in the presented InduMelt reactor (Figure 2) to investigate the achievable transfer coefficients for Li, Ni, Co and Mn under the particular conditions of the reactor. The trend of the measured temperatures in- and outside of the reactor during one of the experiments is presented in Figure 8a. As explained in the materials and methods section, the slope of the outer s-type couples is used to control the temperature inside of the reactor after the operating temperature of the k-type couples is exceeded.

(**a**)　　　　　　　　　　　　　　　　　　　　　　　　(**b**)
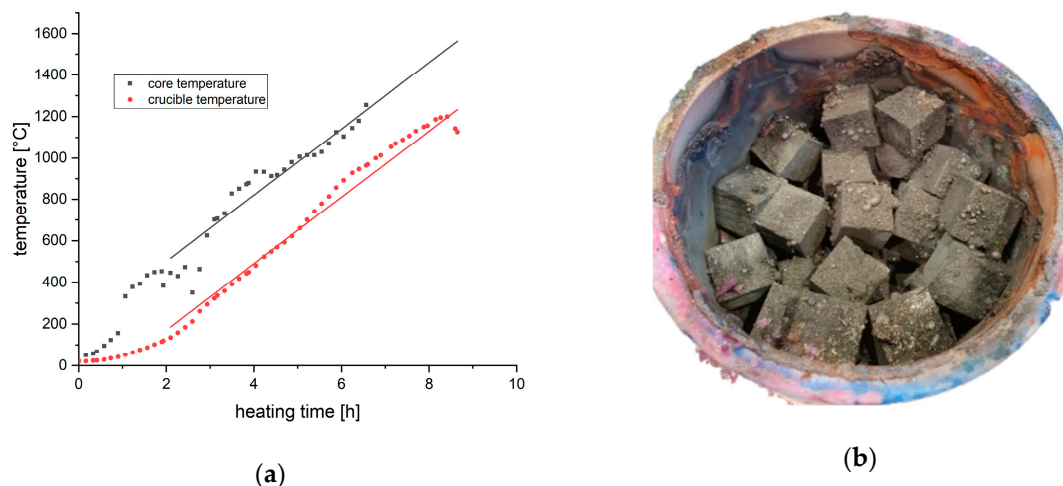
Figure 8. (**a**) Trend of reactor temperatures during IM_NMC_C. (**b**) Picture showing the crucible and the packed bed of graphite cubes with metal depositions after IM_NMC_C.

In Table 2 the compositions of the input mixtures for the InduMelt experiments are shown. For NMC_C and NCA_C the composition matches the stochiometric proportion of the used cathode materials (NCA, $LiNi_{0.8}Co_{0.15}Al_{0.05}O_2$; NMC, $LiNi_{0.33}Mn_{0.33}Co_{0.33}O_2$) with carbon addition of 10 w/%. If the whole added carbon is used and all oxides are removed the mass loss should accumulate to 40–46% of the input mass depending on

the amount of Li that can be removed. For AM, which is a mixture of different cathode materials from LIBs and considering its composition most likely also other battery types, the volatile components also accumulate to around 42 w/%.

Table 2. Chemical composition of the input mixtures for the InduMelt experiments. (w/%).

Sample/Element	Li	Ni	Mn	Co	Al	O_2	C	Sum
AM	2.42	20.90	1.08	4.19	5.83	11.16 [2]	29.50	75.08 [1]
NCA_C	6.50	43.98	0.00	8.28	1.26	29.97	10.00	100.00
NMC_C	6.48	18.25	17.09	18.33	0.00	29.85	10.00	100.00

[1] Cu and other impurities are not specified here since they are not in focus of the experimental series. [2] Calculated on basis of the stochiometric Li-O_2 ratio.

Because the aim of the experimental series is to investigate possible recovery and removal rates for certain metals contained in the cathode materials, Cu and other impurities of the sample AM are not further analyzed.

For the first InduMelt experiments with LIB cathode materials and black matter a maximum temperature of approx. 1550 °C was chosen. At this temperature, no further changes of the CSA or mass during the STA and heating microscope were observed and the expected metal alloy's melting point is also some ten degrees lower. This temperature was then held for approx. one hour before the heat input was stopped.

In Figure 8b the reactor after the experiment is shown. All graphite cubes were removed and cleaned from metal and slag deposits which were subsequently weighed. The individual mass of input material and product phases for each experiment can be seen from Table 3.

Table 3. Masses of the input sample and the obtained products in InduMelt experiments. (g).

Experiment/Product	Input	Metal phase	Slag Phase	Powder	Product Sum
IM_NMC_C	552.3	244.2	37.7	11.6	293.5
IM_NCA_C	520.0	267.3	21.6	15.6	304.5
IM_AM [1]	561.9	-	-	396.1	396.1

[1] Neither metal accumulations nor slag depositions could be found.

The obtained product phases are subdivided into metal phase, slag phase and powder. On the first look at Table 3, one can see that the product distribution differs greatly between the experiments IM_NMC_C, IM_NCA_C and the experiment IM_AM. Therefore, the results are presented and discussed separately.

For IM_NCA_C and IM_NMC_C the metal and slag phase accumulates at the bottom of the reactor or can be found as depositions on the graphite cubes and the crucible. To achieve the best mass balance possible, the depositions have been rubbed of the graphite cubes and the metal particles were magnetically separated. By this, 244.2 g respectively 267.3 g of a metal product, which—if we assume that the metal phase only consists of Ni, Co and Mn—accounts for 81% and, respectively, 91% of the said metals in the input material of IM_NMC_C and IM_NCA_C. According to the oxygen potentials of the metals, the slag phase should mainly consist of Li_2O and Al_2O_3. With 37.7 g and 21.6 g of obtained slag for IM_NMC_C and IM_NCA_C compared to an input of approximately 36 g of pure Li alone one can say that this result looks promising, since the amount of oxygen—and of course Al—must also be taken into account. Furthermore, the refractory mortar and the crucible material also consist of Al_2O_3 and can take part in the reactions causing slag formation. Because this discussion is more complex than for the metal phase it will be continued later together with the chemical analyses of the phases. The powder phase of IM_NMC_C and IM_NCA_C is caused by abrasion during the removal of the small metal particles from the graphite cubes and therefore mainly consists of carbon. Summarized, the overall weight loss of IM_NMC_C and IM_NCA_C is 46.8% and, respectively, 41.4% of the input mass. If we assume that Li, O and C are the only volatile components in the

input material a maximum weight loss of 47.2% for IM_NMC_C and 50.2% for IM_NCA_C is achievable. For IM_NMC_C, the obtained slag phase is shown in Figure 9a, the metal accumulation in Figure 9b.
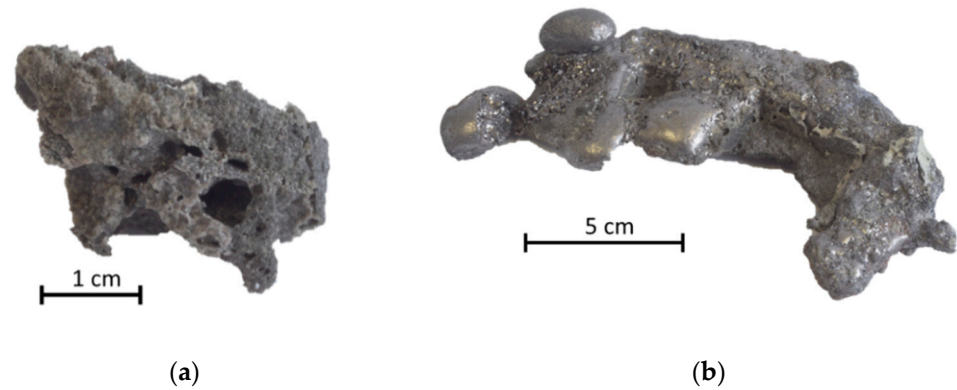

(**a**) (**b**)

Figure 9. Obtained slag (**a**) and metal sample (**b**) from the experiment IM_NMC_C.

As can be seen, the separation of the metal and slag phase in IM_NMC_C for further chemical analysis was relatively easy since large specimens without fusions could be found. In contrast, the obtained products from IM_NCA_C were harder to separate as Figure 10a–d shows. Therefore, the ICP-MS analysis was performed for both, samples with and without inclusions, and the results weighted during data evaluation.
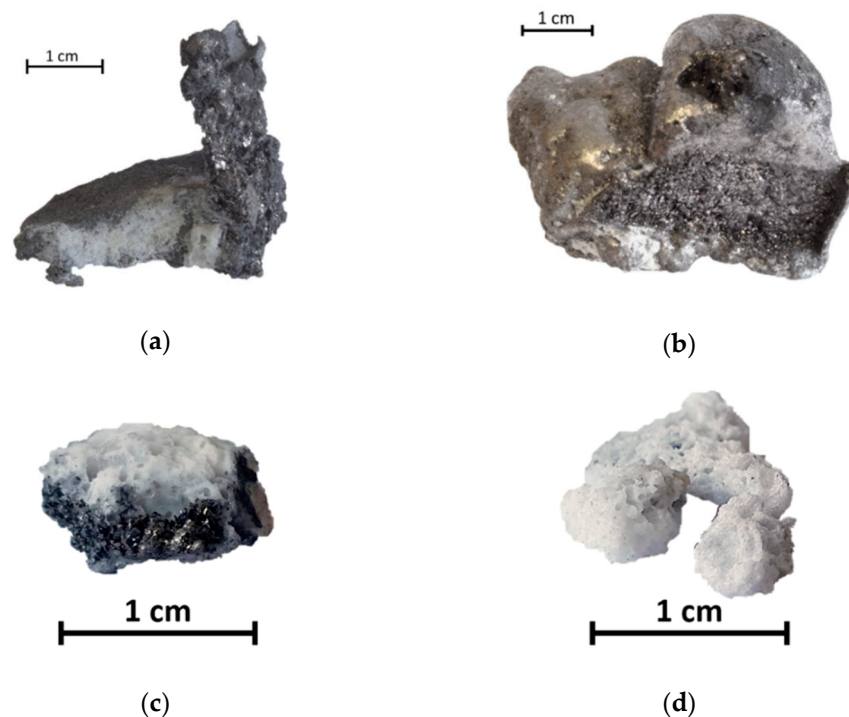

(**a**) (**b**)

(**c**) (**d**)

Figure 10. Obtained metal and slag samples from the IM_NCA_C experiment. (**a**) Metal sample 1 which is strongly fused with the produced slag. (**b**) Metal sample 2 with very little slag inclusions. (**c**) Slag sample 1 with metal depositions. (**d**) Slag sample 2 without inclusions or depositions.

To intensify this discussion, we need to look at the results of the chemical analysis, which were achieved by ICP-MS analysis. The discussion starts with the obtained metal phase from the experiments IM_NMC_C and IM_NCA_C for which the results are contained in Table 4.

Table 4. Mass fractions of certain metals in the obtained metal phases. (w/%).

Experiment/Species	Li	Ni	Co	Mn	Al
IM_NMC_C	0.09	38.40	36.10	28.10	0.01
IM_NCA_C_1 [2]	1.31	74.70	7.80	[1]	3.70
IM_NCA_C_2 [3]	0.05	92.20	9.89	[1]	[1]

[1] Species was not analyzed in this experiment. [2] Small inclusions of slag in the metal matrix need to be considered. [3] Slightly over-determined due to weighted consideration of residuals from the aqua regia digestion.

For IM_NMC_C the metal composition mostly matches the expected result. There is almost no Li and Al present in the metal alloy but Ni, Co and Mn. What is noticeable, however, is the significantly lower Mn content compared to Ni and Co. With an equal stoichiometric proportion and similar molecular weight—Mn is a little lighter—the difference should not be that high, which indicates that Mn also accumulates somewhere else than in the metal alloy.

As already explained, the sampling of NCA_C was not trivial due to small slag inclusions within the metal particles. In order to increase the informative value, metal samples with (IM_NCA_C_1) and without (IM_NCA_C_2) small slag particles were analyzed. By this it can be stated that also for IM_NCA_C there was hardly an accumulation of Li and Al in the metal alloy that mainly consists of Ni and Co.

A complete mass balance is hardly feasible due to the difficult collection of the small metal particles. In future experiments and respective analyses, ICP-OES as well as XRD analysis methods will be used to balance all the elements included in greater detail. Nevertheless, compared to the initial amount in the input material it was possible to find around 90% of Ni and Co and 76% of Mn in the metal phase of IM_NMC_C as well as more than 90% of Ni and Co in the metal phase of IM_NCA_C.

In order to investigate the whereabouts of Mn, to clarify whether Ni and Co can also be found in the slag and to finally check the question of whether Li removal from the reactor could be achieved or not we now look at the slag analysis shown in Table 5.

Table 5. Mass fractions of certain metals in the obtained slag phase. (w/%).

Experiment/Species	Li	Ni	Co	Mn	Al
IM_NMC_C	8.22	0.13	3.06	0.15	6.08
IM_NCA_C_1	9.85	1.31	[1]	[1]	7.45
IM_NCA_C_2	4.52	0.24	0.03	[1]	2.48

[1] Species was not analyzed in this experiment.

Beginning with IM_NMC_C it can be said that Ni does hardly accumulate in the slag while a significantly higher but still low amount of Co could be found. For Mn, from which only 76% of its initial input were found in the metal phase, can also not be found in the slag phase. Since Mn is very reactive and has several oxidation states it is likely that parts of it were removed from the reactor via the gas phase. For IM_NMC_C, analogous to the metal phase results, there are again two samples, IM_NCA_1 with metal particles and IM_NCA_2 without metal particles. The data shows that only a small amount of Ni and Co is found in the slag while Li and Al accumulate to higher extents.

If we now compare the amount of Li that was initially inserted in the experiments, which was approx. 36 g for IM_NCA_C and IM_NMC_C with the amount of Li that was found in the metal and slag phase, a lithium removal of 96.72 w/% for IM_NCA_C and 90.76 w/% for IM_NMC_C was achieved.

Before these results are finally summarized, we have to take a look at IM_AM, which, as mentioned at the beginning, behaved differently than IM_NCA_C and IM_NMC_C. As can be seen in Table 3, neither a metal nor a slag accumulation was found but only a fine powder that was optically identical to the input material. The weight loss of 29,5% matches the initial carbon content exactly, which at first sight suggests that only the included carbon was burned in the reactor. However, analysis of the carbon content of the resulting powder

revealed a mass content of still 22.6%, which indicates that also in IM_AM reduction reactions occurred. In the thermogravimetric analyses only a decrease in mass of 10% was achieved. This could be an indication that certain reactions proceed more slowly in AM and that longer holding times in the preliminary experiments would have provided better results, which is going to be investigated in the further course of the project. Furthermore, an increase of the average particle size was found that indicates at least an agglomeration of particles even if there was no molten phase. Because there was no slag or metal phase in IM_AM, the results are discussed by a comparison of the chemical composition before and after the InduMelt experiment, which is shown in Table 6.

Table 6. Chemical composition of AM before and after the InduMelt experiment. (w/%).

Experiment/Species	Li	Ni	Co	Mn	Al
AM before IM [1]	2.42	20.90	4.19	1.08	5.83
AM after IM [2]	0.77	35.00	7.00	1.76	4.12

[1] Total mass of input material: 561.9 g. [2] Total mass of product: 396.1 g.

The mass content of Ni, Co and Mn has risen by about 65% each which can only be caused by the mass loss of the sample. A statement about a possible discharge of Mn via the gas phase, as it was observed in IM_NMC_C, should not be made due to the already low concentration in IM_AM. Lithium had an input mass of 13.59 g and was reduced to 3.04 g in the product powder, which corresponds to a decrease of 77.6 w/%. This value is significantly lower than with pure cathode materials but in the light of the different behavior of AM compared to NCA_C and NMC_C in all experimental series still a promising result.

To finally summarize the InduMelt experiments, one must notice that the difficulties to achieve a complete mass balance and the absence of an off-gas analysis lead to the fact that the absolute numbers should only be considered to a limited extent. However, it is not the claim of this work to precisely define transfer coefficients for all species in cathode materials respectively black matter, but to evaluate the magnitude of possible recovery rates for the valuable metals Ni, Co, Mn and Li by using the InduRed reactor technology. In view of this, these tendencies are summarized in Figure 11.
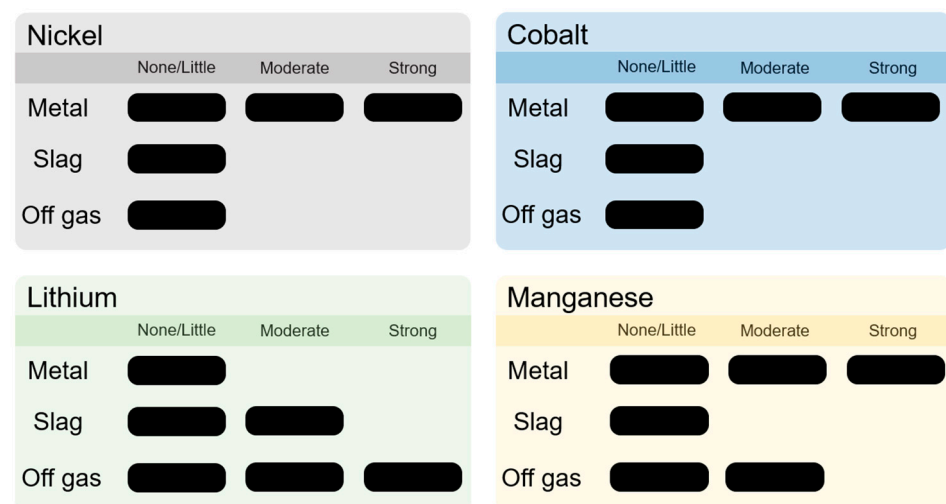

Figure 11. Qualitative consideration of the accumulation of Ni, Co, Mn and Li in the product phases obtained from the InduMelt experiments.

4. Conclusions

The literature research clearly shows that the possibility of simultaneous lithium recovery with a pyrometallurgical process would close a large gap in the recycling chain.

To evaluate if the presented InduRed technology can potentially provide a solution to this problem, a series of experiments have been conducted. By heating microscope experiments and simultaneous thermal analysis, the behavior of NCA and NMC cathode materials as well as black matter (AM) at high temperatures and under reducing conditions was investigated. The results showed that the significant reduction reaction between the lithium metal oxides and carbon take place between 800 °C and 1000 °C and that the produced metal alloy melts at approximately 1500 °C, which are technically feasible temperatures for the desired process.

Experiments, conducted in the InduMelt plant, a lab scale reactor modeled on the InduRed concept, were used to evaluate the transfer coefficients of Ni, Co, Mn and Li in qualitative terms. It was shown that Ni and Co seem to be fully recoverable by this technology while parts of manganese are removed from the reactor via the gas phase. For Li, which is considered to be the bottleneck of pyrometallurgical LIB recycling approaches, very promising results have been seen. In the InduMelt experiments with NCA and NMC more than 90%, respectively more than 75% in the experiment with black matter, of the initial Li were removed from the reactor. The fact that Li does neither accumulate in the slag nor in the metal phase indicates a high potential of the technology to enable new possibilities for Li recovery from the LIB waste stream. If Li is not obtained in small amounts in a slag phase, as in other processes, but can be collected in a separate material flow, its recovery from there can potentially be achieved with less effort and therefore represented more economically.

In order to better examine the removal of Li and Mn from the reactor, the experiments are going to be repeated using a gas vent with gas scrubbing. This should clarify in which form the Li can be obtained from the exhaust gas and how its recovery from there could be achieved. Furthermore, new cathode materials like NMC in other configurations (811, 622, 532 instead of 111) as well as LFP (lithium iron phosphate) are planned to be investigated regarding their suitability for treatment in the InduRed reactor.

The results from experiments with black matter (AM) showed some significant differences, which could partly be attributed to residues from the pre-treatment or excessively high temperatures during the thermal deactivation. Since the contrary behavior of AM in all experimental series cannot be fully elucidated with the available data, further research and experiments are necessary. In addition to that, it is planned to investigate black matter from different pre-treatment processes and the influence of interfering species like Cu or Al in general.

Author Contributions: Conceptualization, S.W.-K. and A.H.; methodology, S.W.-K.; investigation, S.W.-K., A.H. and C.P.; resources, S.W.-K., A.H. and C.P.; writing—original draft preparation, S.W.-K. writing—review and editing, S.W.-K., A.H., C.P. and H.R.; visualization, S.W.-K.; supervision, C.P. and H.R.; project administration, C.P.; funding acquisition, H.R. All authors have read and agreed to the published version of the manuscript.

Institutional Review Board Statement: Not applicable.

Informed Consent Statement: Not applicable.

Data Availability Statement: The data presented in this study are available on request from the corresponding author.

Conflicts of Interest: The authors declare no conflict of interest.

References

1. Mizushima, K.; Jones, P.C. LixCoO$_2$ (0 <x <−1): A new cathode material for batteries of high energy density. *Mater. Res. Bull.* **1980**, *6*, 783–789.
2. Li, L.; Zhang, X. The Recycling of Spent Lithium-Ion Batteries: A Review of Current Processes and Technologies. *Electrochem. Energy Rev.* **2018**, *4*, 461–482. [CrossRef]
3. Ding, Y.; Cano, Z.P. Automotive Li-Ion Batteries: Current Status and Future Perspectives. *Electrochem. Energy Rev.* **2019**, *1*, 1–28. [CrossRef]

4. Berckmans, G.; Messagie, M. Cost Projection of State of the Art Lithium-Ion Batteries for Electric Vehicles Up to 2030. *Energies* **2017**, *10*, 1314. [CrossRef]

5. Arambarri, J.; Hayden, J. Lithium ion car batteries: Present analysis and future predictions. *Environ. Eng. Res.* **2019**, *4*, 699–710. [CrossRef]

6. Redux Smart Battery Recycling. Available online: https://www.redux-recycling.com/de (accessed on 28 December 2020).

7. Umicore Battery Recycling. Available online: https://csm.umicore.com/en/battery-recycling/e-mobility (accessed on 28 December 2020).

8. Lithium Batterie Recycling. Available online: https://accurec.de/lithium?lang=de (accessed on 28 December 2020).

9. Battery Recycling Datasheet. Available online: https://accurec.de/wp-content/uploads/2018/04/Li-ion-RE_2018.pdf (accessed on 28 December 2020).

10. Arnberger, A.; Coskun, E. Recycling von Lithium-Ionen-Batterien. In *Recycling und Rohstoffe*; Thiel, S., Thomé-Kozmiensky, E., Eds.; TK Verlag: Nietwerder, Germany, 2018; pp. 583–599.

11. Werner, D.; Peuker, U.A. Recycling Chain for Spent Lithium-Ion Batteries. *Metals* **2020**, *3*, 316. [CrossRef]

12. Liu, C.; Lin, J. Recycling of spent lithium-ion batteries in view of lithium recovery: A critical review. *J. Clean. Prod.* **2019**, *228*, 801–813. [CrossRef]

13. Mishra, D.; Kim, D.-J. Bioleaching of metals from spent lithium ion secondary batteries using *Acidithiobacillus ferrooxidans*. *J. Waste Manag.* **2008**, *28*, 333–338. [CrossRef]

14. Xin, Y.; Guo, X. Bioleaching of valuable metals Li, Co, Ni and Mn from spent electric vehicle Li-ion batteries for the purpose of recovery. *J. Clean. Prod.* **2016**, *116*, 249–258. [CrossRef]

15. Zeng, G.; Deng, X. A copper-catalyzed bioleaching process for enhancement of cobalt dissolution from spent lithium-ion batteries. *J. Hazard. Mater.* **2012**, *199*, 164–169. [CrossRef]

16. Zeng, G.; Luo, S. Influence of silver ions on bioleaching of cobalt from spent lithium batteries. *Miner. Eng.* **2013**, *49*, 40–44. [CrossRef]

17. Bahaloo-Horeh, N.; Mousavi, S.M. Use of adapted metal tolerant Aspergillus niger to enhance bioleaching efficiency of valuable metals from spent lithium-ion mobile phone batteries. *J. Clean. Prod.* **2018**, *197*, 1546–1557. [CrossRef]

18. Ghassa, S.; Farzanegan, A. Novel bioleaching of waste lithium ion batteries by mixed moderate thermophilic microorganisms, using iron scrap as energy source and reducing agent. *Hydrometallurgy* **2020**, *197*, 105465. [CrossRef]

19. Heydarian, A.; Mousavi, S.M. Application of a mixed culture of adapted acidophilic bacteria in two-step bioleaching of spent lithium-ion laptop batteries. *J. Power Sources* **2018**, *378*, 19–30. [CrossRef]

20. Vest, M. Weiterentwicklung des Pyrometallurgischen IME Recyclingverfahrens für Li-Ionen Batterien von Elektrofahrzeugen. Ph.D. Thesis, RWTH Aachen, Aachen, Germany, 28 January 2016.

21. He, L.-P.; Sun, S.-Y. Recovery of Lithium, Nickel, Cobalt, and Manganese from Spent Lithium-Ion Batteries Using l -Tartaric Acid as a Leachant. *ACS Sustain. Chem. Eng.* **2017**, *5*, 714–721. [CrossRef]

22. Elwert, T.; Frank, F. 2020, Auf dem Weg zu einem geschlossenen Stoffkreislauf für Lithium-Ionen-Batterien. In *Recycling und Sekundärrohstoffe*; Thomé-Kozmiensky, E., Holm, O., Eds.; TK Verlag: Neuruppin, Germany, 2018; pp. 525–530.

23. Huang, B.; Pan, Z. Recycling of lithium-ion batteries: Recent advances and perspectives. *J. Power Sources* **2018**, *399*, 274–286. [CrossRef]

24. Yin, H.; Xing, P. Pyrometallurgical Routes for the Recycling of Spent Lithium-Ion Batteries. In *Recycling of Spent Lithium-Ion Batteries*; Liang, A., Ed.; Springer International Publishing: Cham, Switzerland, 2019; Volume 4, pp. 57–83.

25. Gao, R.; Xu, Z. Pyrolysis and utilization of nonmetal materials in waste printed circuit boards: Debromination pyrolysis, temperature-controlled condensation, and synthesis of oil-based resin. *J. Hazard. Mater.* **2019**, *364*, 1–10. [CrossRef]

26. Beheshti, R.; Tabeshian, A. Lithium-Ion Battery Recycling Through Secondary Aluminum Production. In *Energy Technology*; Zhang, L., Jaroslaw, W., Eds.; Springer International Publishing: Cham, Switzerland, 2017; pp. 267–274.

27. Dorella, G.; Mansur, M.B. A study of the separation of cobalt from spent Li-ion battery residues. *J. Power Sources* **2007**, *170*, 210–215. [CrossRef]

28. Schönberg, A. Mathematische Modellierung metallurgischer Prozesse—Induktive Erwärmung einer Graphitschüttung. Ph.D. Thesis, Montanuniversität Leoben, Leoben, Germany, 11 December 2014.

29. Ponak, C. Carbo-Thermal Reduction of Basic Oxygen Furnace Slags with Simultaneous Removal of Phosphorus via the Gas Phase. Ph.D. Thesis, Montanuniversität Leoben, Leoben, Germany, 2 September 2019.

30. Ponak, C.; Mally, V. Phosphorus Gasification during the Reduction of Basic Oxygen Furnace Slags in a Novel Reactor Concept. *Adv. Mater. Lett.* **2020**, *11*, 20071535. [CrossRef]

31. Mao, J.; Li, J. Coupling reactions and collapsing model in the roasting process of recycling metals from $LiCoO_2$ batteries. *J. Clean. Prod.* **2018**, *205*, 923–929. [CrossRef]

32. Kwon, O.; Sohn, I. Fundamental thermokinetic study of a sustainable lithium-ion battery pyrometallurgical recycling process. *Resour. Conserv. Recycl.* **2020**, *158*, 104809. [CrossRef]